Interfacial Polarization and Ionic Structure at the Ionic Liquid-Metal Interface Studied by Vibrational Spectroscopy and Molecular Dynamics Simulations

Matthew J. Voegtle,[†] Tanmoy Pal,[‡] Anuj K. Pennathur,[†] Sevan Menachekanian,[†] Joel G. Patrow,[†] Sohini Sarkar,[†] Qiang Cui,[‡] and Jahan M. Dawlaty[*,†]

[†]*Department of Chemistry, University of Southern California*

[‡]*Department of Chemistry, Boston University*

E-mail: dawlaty@usc.edu

Phone: 213-740-9337

Abstract

Ionic Liquids (ILs) have both fundamental and practical value in interfacial science and electrochemistry. However understanding their behavior near a surface is challenging due to strong Coulomb interactions, and large and irregular ionic sizes which affect both their structure and energetics. To understand this problem we present a combined experimental and computational study using a vibrational probe molecule, 4-mercaptobenzonitrile, inserted at the junction between a metal and a variety of ILs. The vibrational frequency of the nitrile in the probe molecule reports on the local solvation environment and electrostatic field at this junction. Within the ethylmethyl imidazolium ($EMIM^+$) cation family of ILs, we varied the anions over a range of sizes and types. Complementing our surface spectroscopy, we also ran molecular dynamics simulations of these interfaces to better understand the ionic structures that produced the measured fields. The magnitude of the frequency shifts, and thereby fields, shows a general correlation with the size of anions, with larger anions corresponding to smaller fields. We find that the source of this correlation is partial intercalation of smaller anions into the probe monolayer, resulting into tighter packing of ionic layers near the surface. Larger anions reduce the overall lateral ion packing density near the surface, which reduces the net charge per unit area and explains the smaller observed fields. The insight from this work is important for developing a fundamental picture of concentrated electrolytes near interfaces and can help with designing ILs to create tailored electric fields near an electrode.

Introduction

Ideal room temperature ionic liquids (ILs) are liquid organic salts with relatively mobile anions and cations. They have opened and continue to open new frontiers in applications[1,2] such as in batteries, fuel cells, solar cells, electrochemistry,[3] and ionic thrusters for propulsion in space missions[4] due to their unique properties, including electrochemical and thermal stability, low vapor pressure, and the ability to dissolve a wide range of substances. Most of

these applications rely upon understanding and engineering the behavior of ILs at interfaces with other materials.[5,6] However, their behavior at an interface is often a far cry from the dilute electrolyte interfaces. A few of the central differences are highlighted below.

They have strong Coulomb correlations. Even in a concentrated conventional electrolyte (e.g. 1 M aqueous HCl) the ratio of ions to solvent molecules are in the order of $\sim$ 1:50. In a pure IL the entire liquid is made of ions and strong interaction between ions can not be ignored. For example, ion pairing can change the essential properties that are of value to applications such as conductivity, viscosity, and interfacial kinetics. The degree of ion-pairing in ILs, especially near an interface is a subject of current research.[5,7] Ionic liquids may be thought of as "liquid plasma" and have even been suggested as a test bed for understanding the complexities of plasma physics theories.[8–10] Furthermore, the ions have non-negligible sizes, and size difference between the cations and anions can vary largely. This leads to complex structure formation near the interface. Coulomb interactions compete with other specific intermolecular forces such as hydrogen bonding, van der Waals, and hydrophobic/hydrophilic interactions. Such competition affects physical properties such as melting point and viscosity. Albeit complicated, changing the composition of the ions can promote or demote the importance of a given interaction and serve as a handle in tuning their properties.

Given the above, it is not surprising that conventional theories of electrolytes near interfaces (analogues of Gouy-Chapman theory and its variants) do not generally hold for ILs. Of the many facets of structure and dynamics of ILs, we are interested in only one: local electric field near a surface, which we argue is complicated, and crucial for many applications of ILs. Experimental and computational work[11–13] has shown the potential profile away from an electrode into the IL is non-monotonic and oscillatory, reflecting the underlying layered structure of ions near the electrode.

Ionic liquids have a vast chemical space.[5,14] Their properties can be tuned by somewhat independent choice of anions and cations, with a variety of sizes and substituent groups,

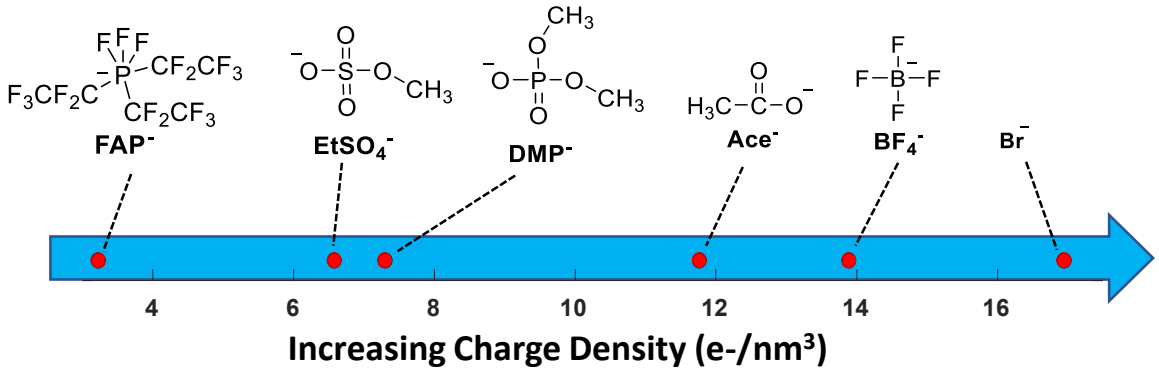

Figure 1: Chemical structure and name abbreviations of the anions studied in this work and their corresponding charge density

leading to millions of possible ILs even by conservative estimates, and thousands already reported in the literature. Rather than randomly searching the parameter space, it is necessary to identify themes and build a general understanding of their behavior at interfaces. In this study, we investigate the surface structure as a function of anion size.

Despite the importance of interfacial fields, their direct experimental measurement is nearly impossible with many conventional techniques. The usual experimental approach is the measurement of differential capacitance as a function of potential. Often such measurements fall under the general umbrella of impedance spectroscopy, in which a static background potential with an added small amplitude oscillatory potential is applied to the interface and the complex response of the interface (consisting of both resistive and capacitive components) is measured as a function of frequency. Then the data is modeled using an *assumed equivalent circuit* for the interface and the capacitance of the interface is inferred. Even if we ignore the inherent reliance of this method on an assumed equivalent circuit model, it is clear that this is a bulk measurement that probes the entire interface and necessarily averages out the intricate field variations near the surface. The interpretation of such measurements for ILs is heavily debated in the literature[15–19] and a clear microscopic picture is yet to emerge. Nonetheless, models and some experiments lead us to believe that even such bulk and averaged out measurement of the interface yields *qualitatively* different results for ILs compared to conventional electrolytes.

Approach

Our work provides a new and independent outlook to this problem by combining a spectroscopic method, Vibrational Sum Frequency Generation (vSFG), with molecular dynamics (MD) simulations. Together, our results provide a detailed view of interfacial structure grounded in experimental observables. To understand the electrostatic polarization of molecules at the metal-IL interface, we measure the nitrile frequency of 4-mercaptobenzonitrile (4-MBN) SAMs adsorbed at the gold surface in the presence of a range of ILs. This molecule is a well-understood vibrational Stark probe and has been used by us and others to probe electric fields at the surface of electrodes.[20–22] Nitrile groups (and other Stark probes) are useful in providing a picture of the local electrostatic environment, but specific interactions such as hydrogen bonding to the nitrile shift the CN frequency in ways that are not explained by a simple mean-field picture.[23–25] More broadly, heterogeneous polarization across the body of the probe complicates the use of Stark spectroscopy for electric field measurements. Electric fields can and do vary over molecular length scales,[26] but the probe only reports a single frequency reflective of an averaged field. Therefore, while the vibrational frequency of the nitrile probe is an important reporter of the local electrstatic environment, it does not imply homogeneity of field at the molecule scale. A molecular scale picture when interpreting vibrational frequencies as arising due to Stark shift is needed. For that reason, we used MD simulations to understand how the measured frequency shifts relate to a detailed picture of the ionic structure at the interface. Using MD simulations, ILs of the imidazolium family have been studied at the interface of vacuum[27–30] and silica.[31,32] Kislenko et al.[33] studied the electrical double layer in $[BMIM]^+[PF_6]^-$ IL at uncharged, positively charged, and negatively charged graphite surfaces. Recently, $[BMIM]^+[BF_4]^-$ in a confined environment between two gold electrode surfaces has been studied.[34]

The frequency shift of nitrile has been used to report the solvation field strength in the bulk of ILs, and the field strength was found to depend on the size of the anion, but little to no dependence on the size of the cations.[35] In this paper, we will refer to the fields reported

by the nitrile probe as interfacial solvation fields. In the spirit of our earlier work, the nitrile probe is effectively solvated by the surrounding ionic environment and the metal which responds both to the probe molecule and the ions. The frequency of the probe responds to the total solvation environment. ILs structure have also been studied extensively by several groups, including those of Baldelli,[36–39] Dlott,[40–42] and Fayer.[43–45] Their work has revealed significant insight into the structure and dynamics of ILs. This work is distinct from the mentioned efforts in that we measure the change in frequency of a Stark reporter, and not the IL itself. In doing so, we gain spatial specificity, since we interact with the Stark probe only in one location, namely near the interface, as opposed to interacting with several layers of liquid, or the bulk of the liquid, all at once.

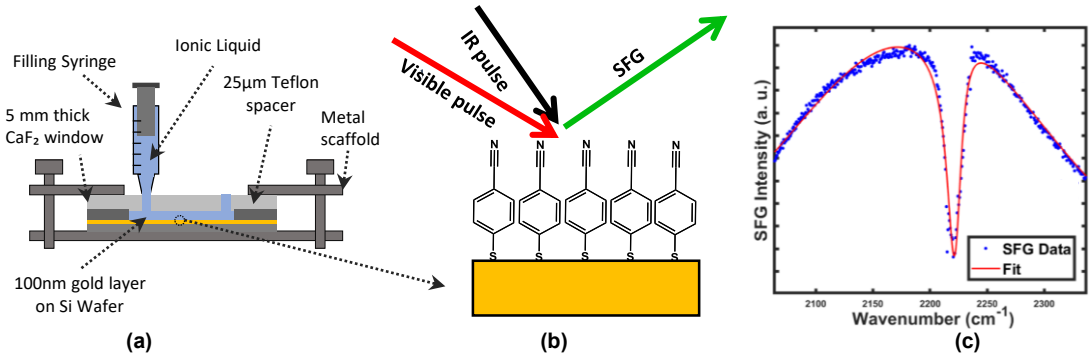

Figure 2: Overview of experimental work. Panel 2a: A diagram of the cell used to acquire SFG spectra. Panel 2b: A cartoon depicting SFG generation from the 4-MBN SAM at the gold-IL interface. Panel 2c: Representative SFG spectra of a 4-MBN SAM showing a broad non-resonant background the narrow CN stretch.

Experimental Methods

Self-assembled monolayers (SAMs) of 4-Mercaptobenzonitrile (4-MBN) were prepared on silicon wafers with a 10 nm Ti adhesion layer and 100 nm of Au purchased from LGA Thin Films, Inc. Wafers were cleaned by sonication in ethanol twice, then in methanol twice for 8 minutes each time, then immersed in a 0.03 M solution of 4-MBN in ethanol overnight. This results in a dense monolayer with full surface coverage for a reproducable spectrum with a

high signal to noise ratio.[46] After soaking in the 4-MBN solution, the wafers were removed and again sonicated in ethanol and then methanol for 8 minutes each.

A 1 kHz regeneratively amplified Ti:Sapph laser (Coherent) was used to generate ultrafast near IR pulses. A portion (1 W) of this was directed to an optical delay stage followed by a 4f filter to significantly narrow the spectrum, while another portion (2 W) was directed to an OPA (Coherent OPerA Solo) equipped with a $AgGaS_2$ crystal for difference frequency generation of mid IR pulses. The 4f filter incorporates two volume phase gratings (BaySpec, Inc), two cylindrical lenses and a variable width slit to filter the near IR pulse to a spectral width of 8.0 cm^{-1}, centered at 784.62 nm. Typical spectra of both the near IR upconversion pulses as well as the broadband mid IR pulses can be found in previous work.[23] Pulse energies were measured at the sample position to be ≈ 8 μJ for the near IR and ≈ 7.56 μJ for the mid IR. VSFG spectra were acquired by focusing these two pulses together on the sample using a parabolic mirror and overlapping them in time. The resulting VSFG signal was collected with a second parabolic mirror and passed through a short pass filter to reject the majority of the scattered near-IR photons.

The SFG was then sent to a spectrometer (Horiba iHR320) with a CCD camera (Sycerity, JY) for spectral analysis. With the input slit of the spectrometer set to 0.05 mm, and using an 1800 gr/mm grating, the theoretically achievable spectral resolution was 0.05 nm (about 1 cm^{-1} in the spectral range of interest), which is well below the width of the near IR upconversion pulse. Spectral resolution of the SFG spectra are, thus, limited by the 8 cm^{-1} width of the near IR upconversion pulses. We point out that peak shifts smaller than this value can be measured as has been discussed in a previous publication.[23]

Vibrational Sum Frequency Generation (VSFG) spectra were taken before and after application of each IL to the gold wafer. Spectra were obtained from three acquisitions, each integrating for 180 seconds. Final raw spectra are a simple average of the three acquisitions. Experiments were conducted in a demountable liquid FTIR cell (International Crystal Laboratories) modified for this purpose (see Figure 2). The back window of the cell was removed

and replaced with the SAM containing wafer and a 25 μm Teflon spacer was placed directly on the sample surface. Ionic liquid was injected into the cell between the gold and a CaF_2 window. The entire assembly is then held firmly together using stainless steel plates and screws. All SFG measurements were taken in a purged environment, free of CO_2 and water. Raw SFG spectra is processed using a fitting equation described by Benderskii et al.,[47] which is comprised of a resonant Lorentzian, a non-resonant Gaussian, and variable phase between the two signals. Temperature dependent SFG measurements were completed using a Lakeshore Model 325 Temperature controller and a Lakeshore DT-670 temperature sensor for temperature measurements. The normal SFG cell was slightly modified with a custom-machined aluminum base which allows for good temperature contact between the heater lead, cell environment and temperature probe. Final data reported from SFG experiments such as center frequencies and line widths are reported from an average of three spectra. Representative SFG spectra for all IL systems studied are reported in the SI (Figure S1).

SERS studies were carried out using a Horiba XploRA Raman Microscope System using a 532 nm fundamental beam. Spectra were taken using a 1800 groove/mm grating in 10 second increments and averaged over six scans. SERS substrates were prepared with the following method, adapted from the literature:[48] A silver strip was sonicated in distilled water for 8 minutes, then submerged in 60% ammonium hydroxide solution for 1 minute, followed by inserting the silver strip in concentrated nitric acid for 10 seconds. The SERS substrates were then sonicated in water again for 8 minutes for a final cleaning before monolayer adsorption. Nitrile peaks from SERS studies were fit to Lorenzians and the error bars shown in the figure are from the 95% confidence interval of the fit. Each IL measurement was taken on a fresh piece of roughened silver and reported frequency shifts represent a subtraction between the 'neat' 4-MBN monolayer and the CN stretch of 4-MBN after application of IL. Raw SERS spectra are reported in the SI (Figure S2).

To investigate the effect of anion size on the surface solvation environment, we used a series of six ILs where the cation identity was fixed and the anion was changed. The cation

used for this series was $[EMIM]^+$. The anions used for this series are —in decreasing size order— tris(pentafluoroethyl)trifluorophosphate (FAP^-), dimethylphosphate (DMP^-), ethyl sulfate ($EtSO_4^-$), acetate (AcO^-), boron tetrafluoride (BF_4^-), and bromide (Br^-). Ionic liquids were purchased from Sigma Aldrich with purities higher than 98%. Structural information of the anions and cations used in this experiment are provided in Figure 1. Ionic liquids were stored under moisture-free air and dried before measurement using a microwave purification method adapted from Ha et al.[49] This method was shown to remove water to levels below 0.5 wt% rapidly and without damage to the ions. In short, aliquots of IL were heated in a lab microwave until IL temperatures reached 120°. We used a Nicolet iS50 FTIR Spectrometer to confirm that this treatment removes water and does not alter IL structure (associated figure is in the SI). The data show that a sample IL is not compromised or damaged by this treatment and that our storage and purification methods result in low water levels.

Computational Methods

The 4-MBN functionalized slab of nanomaterial was generated in the following steps. First, we used CHARMM-GUI[50] nanomaterial modeler to build a 4 nm × 4 nm × 1 nm gold (100) surface with 100 % $-SCH_2CH_3$ ligand coverage (ligand density $\sim 6.25\,nm^2$). An initial energy minimization was performed using the Steepest Descent algorithm in the CHARMM[51] package. Then the system was translated, rotated and minimized again to obtain a 4 nm × 4 nm × 2 nm gold surface with ligands on both positive and negative Z directions. Next, the ethyl part of the ligands was replaced (patched[51]) with 4-benzonitrile group to obtain the 4-MBN functionalized gold slab. Enegy minimization was performed again before packing the system with ILs. Detailed system dimensions and number of ions are included in SI Table S3.

It is well known that consideration of electronic polarization is important for studying

the structure and dynamics of ILs. Electronic polarization is known to reduce enthalpy of vaporization, and accelerate the ion diffusion.[52] Studies have found that diffusion coefficients simulated using non-polarizable force fields are smaller than the experimental values.[53–55] Yan et al.[56] showed that for $[EMIM]^+[NO_3]^-$, introducing electronic polarization increases the diffusion coefficient to three times of non-polarizable model. They also observed that due to higher ion mobility, the shear viscosity calculated from the polarizable model was in better agreement with the experimental values.[56] However, the effect of electronic polarization on IL structure is more subtle,[52] mainly in terms of anion-anion pair correlations.[52,56,57] Polarization is shown to relax long-range ion structuring in $[BMIM]^+[BF_4]^-$, and the influence propagates to short-range ion-ion correlation.[57] The effect of polarization is known to be more pronounced for asymmetric ions.[57] Nevertheless, non-polarizable force fields are shown to reproduce IL structure quite well,[56–60] due to the dominant effect of electrostatics. Since we focus on the trends in structural features across a series of ILs in this study, we use non-polarizable force fields due to their higher computational efficiency and broader range of availability for different ILs.

Unless stated otherwise, non-polarizable CHARMM36[61,62] and CHARMM General Force Field[63–66] were used to describe the ligands and the ILs. Lennard-Jones parameters for Br^- anions were taken from Canongia Lopes et al.[67] The structure of BF_4^- anion was optimized with B3LYP[68–73] and the aug-cc-pVDZ[74] basis set in the Gaussian 16 program.[75] The force field parameters for BF_4^- were taken from de Andrade et al.[76] The authors develop the intra-molecular potential parameters using AMBER methodology,[77] and the Van der Waals parameters for fluorine and boron were sourced from AMBER[78] and DREIDING[79] force fields respectively. The $[DMP]^-$ anion has been modeled using the ligand modeler[80] in CHARMM-GUI.[50] Finally, the geometry of $[FAP]^-$ anion was optimized using the same DFT method and basis set as in BF_4^-. The force field parameters used for $[FAP]^-$ are developed by Shimizu et al.[81] based on the OPLS-AA molecular force field. In our implementation, the harmonic force constant for F-P-F, C-P-F, and C-P-C angles have been increased

to 1000 $KJ\,mol^{-1}\,rad^{-2}$ for additional rigidity around the phosphorus center. The diffusion coefficients calculated in this work (SI Table S4) are of the order of $10^{-11}\,m^2\,s^{-1}$, consistent with previous experimental[82,83] and simulation studies[84–87] The computed densities are also in decent agreement with those reported in previous work (see SI Table S5).

For the gold surface, we use the INTERFACE force field,[88,89] which has been successfully applied to gold surface and gold nanoparticles. This choice is further supported by a recent study from Ntim and Sulpizi,[34] who demonstrated that the density profiles and cation/anion orientation of IL ($[BMIM]^+[BF_4]^-$) was negligibly affected by gold polarization.

The functionalized surface was packed with 550-1130 pairs of different IL cations and anions, and molecular dynamics simulations were performed using the GPU version of the GROMACS[90–96] 2018 package. Position restraints of 200,000 $KJ\,mol^{-1}\,nm^{-2}$ were applied on the gold atoms in all three dimensions. Periodic boundary conditions were employed in three dimensions as well. After energy minimization, the systems were equilibrated for 100 ps in the NVT ensemble (with 0.5 fs timestep), and 200 ns in the NPT ensemble (with 2 fs timestep). 200 ns of production run was performed thereafter, with a timestep of 2 fs.

The particle-mesh-Ewald[97] method with a Fourier spacing of 0.12 nm was used to calculate electrostatic interactions. Real space non-bonded interactions were treated with a cut-off distance of 1.2 nm and a force-switch modifier. LINCS[98,99] algorithm was used to constrain all bonds involving hydrogen atoms.

We used the Berendsen[100] thermostat with a time constant of 1 ps and a target temperature of 400 K for equilibration NPT runs, and the Nosé-Hoover[101,102] thermostat with same parameters for production runs. Semi-isotropic pressure coupling was applied for all NPT simulations with a target pressure of 1.0 atm. The Berendsen[100] pressure-coupling scheme with a time constant of 5.0 ps and compressibility of $4.5 \times 10^{-5}\,bar^{-1}$ was used for equilibration, while we used the Parrinello-Rahman[103,104] method with a time constant of 10.0 ps and compressibility of $4.5 \times 10^{-5}\,bar^{-1}$ for production simulations.

To probe local electrostatics at the interface, we calculate the electric field at the nitrile

nitrogen of the 4-MBN probe. The electrostatic field at position $\mathbf{r}$ due to point charges q_i at positions $\mathbf{r_i}$ is given by:

$$\mathcal{E}(\mathbf{r}) = \sum_{i=1}^{n} q_i \frac{(\mathbf{r} - \mathbf{r}_i)}{|\mathbf{r} - \mathbf{r}_i|^3} \quad (1)$$

In this study, an atom-based cut off distance of 3.5 nm is used for field calculation. The choice of cut-off distance is based on the convergence of electric field components to $10^{-2}\, V\, nm^{-1}$ (SI Figure S9). We calculate the electric field exclusively from ILs, and it's projection along C-N axis for all 200 nitrile nitrogens. The electric field is sampled every 50 ps for the last 100 ns of production run. (Histograms of electric field components and projection are shown in SI Figures S10, S11). At that timescale, the components and the projection of electric field are decorrelated (SI Figure S12). The component of the electric field on nitrile nitrogens along C-N is averaged over space and time, and is used next to calculate the estimated Stark frequency shift. Assuming a linear Stark tuning rate of $\Delta\vec{\mu} = 0.36\, cm^{-1}(MV/cm)^{-1}$ for benzonitriles,[21,105–110] we report the estimated Stark frequency shift $\Delta\nu_{CN}$(SI Figure 5a, 5b).

The volume of anions was estimated using the quantum chemistry package QChem 5.1.[111] Anion structures were optimized using the B3LYP functional and the 6-31G* basis set. Following optimization, the volume corresponding to 99% of the anion's electron density was extracted from the cube file associated with the final structure. The volumes estimated by this method match those published in work by others.[35]

Results

We first present experimental results showing the dependence of the probe vibrational frequency on the anion charge density, followed by computational results confirming the experimental trend. Figure 3a shows the extracted Lorenzian fits to the nitrile SFG spectra, with the dotted line representing the nitrile frequency of the monolayer in contact with air (see

SI for details). All center frequency shifts with respect to air are plotted in Figure 3b. Our main result is the observation of a systematic shift in the central frequency with decreasing anion size (i.e. increasing charge density). Over the range of ILs studied, we observe the smallest nitrile shift ($\sim$2 cm^{-1}) from the IL with the largest anion ($[EMIM]^+[FAP]^-$), and the largest shift ($\sim$12.5 cm^{-1}) from the IL with the smallest anion ($[EMIM]^+[Br]^-$). Under the assumption of a linear Stark tuning rate (discussed in our previous work),[20] this corresponds to a considerable interfacial solvation field of $\sim$3.6 V/nm. The reason for this behavior could only be explained after our MD simulations, revealing a structure arising from a balance between size, ion packing and electrostatics near the surface, as will be explained in the discussion section below.

Because frequencies extracted from SFG are inherently convoluted with a non-resonant background and are highly dependent on reliable fitting,[112] we supplemented the SFG measurements with surface-enhanced Raman spectroscopy (SERS). Though the roughened surfaces required for SERS introduce additional complexity,[113,114] it can still serve as a useful comparison and alleviates concerns regarding phase-amplitude mixing in recovering the SFG central frequencies. Our measured SERS results (shown in Figure 4) are generally in agreement with the SFG results and the overall trend with respect to anion size is consistent between the two. The agreement between these two experimental techniques indicates that $\Delta\nu_{CN}$ values extracted from SFG are not significantly impacted by fitting and background errors, thereby confirming the observed trend in frequencies with respect to anionic charge density.

As an additional experimental check, the temperature dependence of the benzonitrile monolayer's CN stretch in ($[EMIM]^+[Br]^-$) was measured using VSFG. Varying the temperature from 295K to 380K did not change the nitrile center frequency greater than an approximate bounds of $\pm$0.5 cm^{-1}. The results of this experiment are shown in Figure S4. This confirms that the ionic structures studied, at least in the range of temperatures studied, are not in a metastable configuration and represent an equilibrium arrangement.

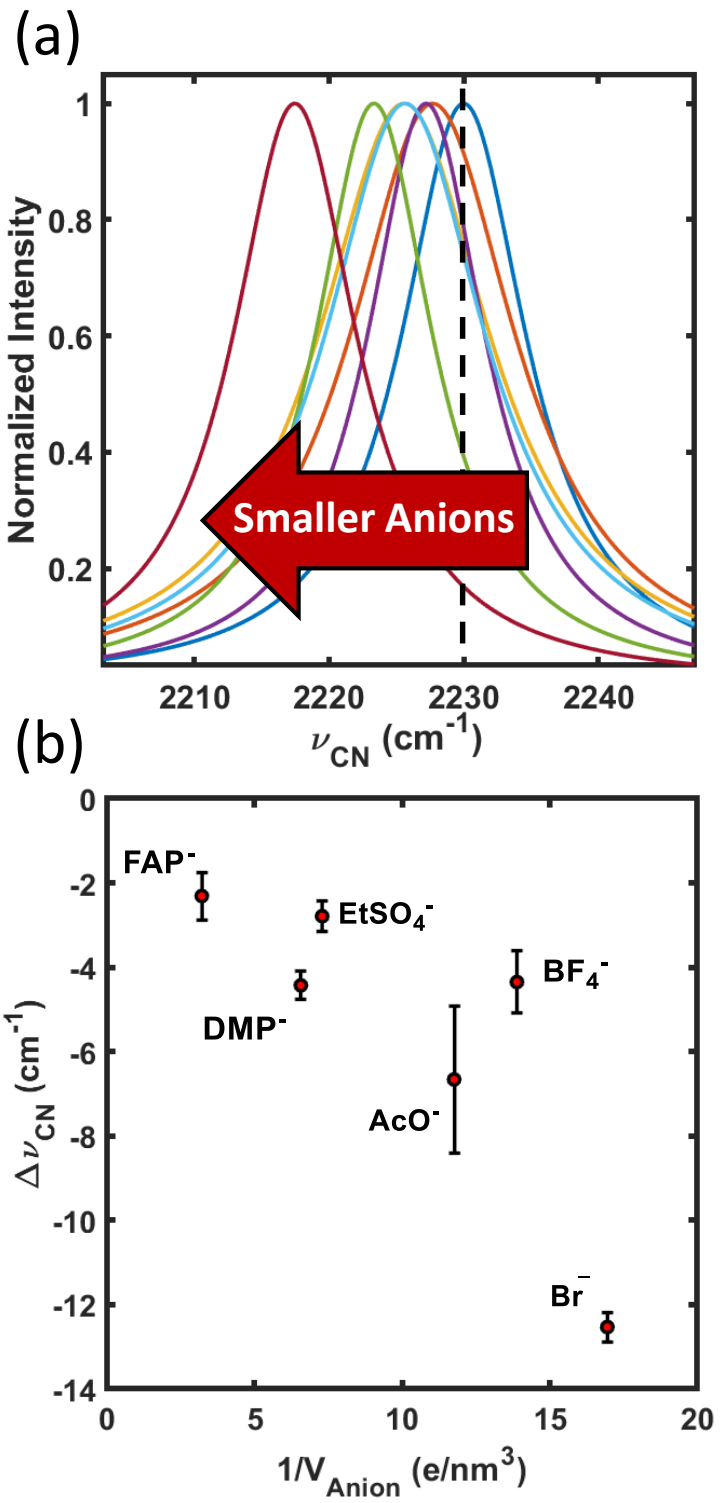

Figure 3: Room temperature frequency shifts of 4-MBN monolayer on the electrode surface in the presence of different ILs. Figure 3a shows extracted Lorenzians from raw SFG spectra, and Figure 3a shows the center nitrile frequency plotted against the charge density of the anion. The monolayer is strongly solvated in the presence of smaller anions, with a large field of ~3.6 V/nm observed using $[EMIM]^+[Br]^-$.

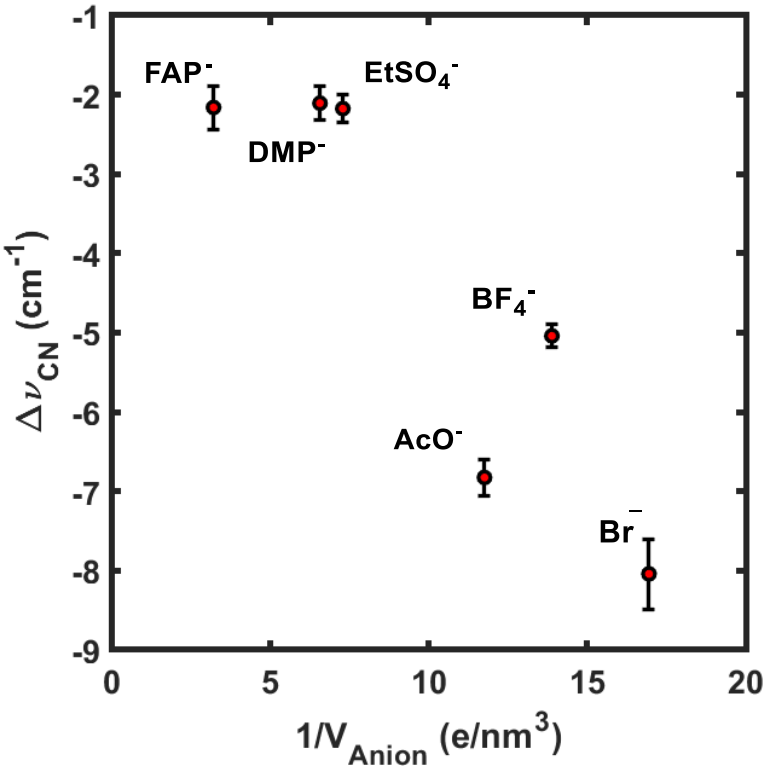

Figure 4: Surface enhanced Raman (SERS) data of the nitrile center frequency in the presence of different ILs. Chemically etched silver was used as a substrate. We observe an increase in polarization at the interface correlated with smaller anion size, in agreement with the SFG results. Point to point differences between SERS and SFG measurements may be related to heterogeneity at the SERS surface.

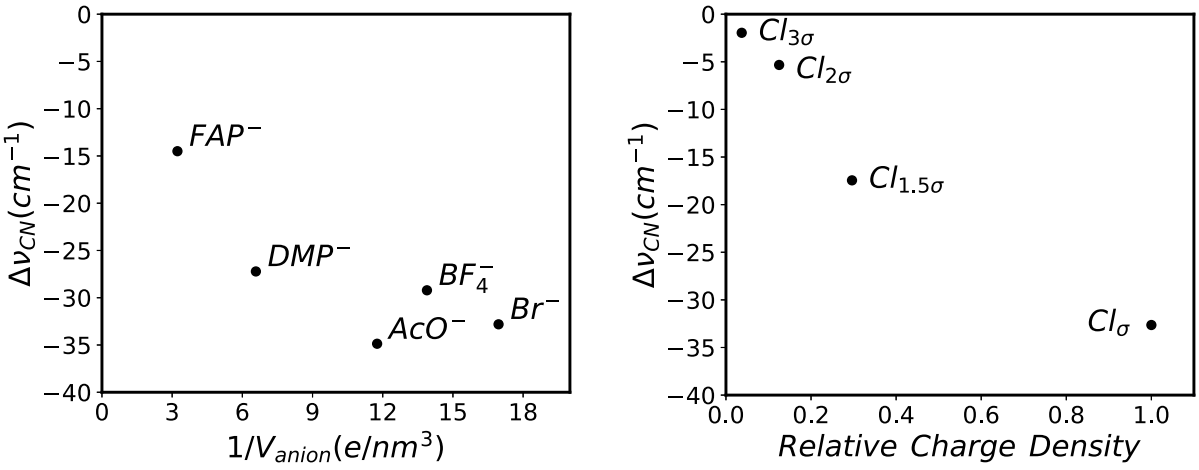

(a) (b)

Figure 5: Calculated frequency shifts at nitrile carbon of 4-MBN monolayer on the gold slab in presence of different ILs. (a) Realistic anions with $[EMIM]^+$ cations, and (b) Modified Cl^- anions with $[EMIM]^+$ cations. Lennard-Jones σ for $Cl^- = 4.04\,\text{Å}$.

The computational results comprise of two parts. First, the calculated frequency shift of the probe molecule in the presence of an equilibrated configurational ensemble of ILs, and second, analysis of the arrangement of ions as a function of distance from the surface.

Following procedures explained in the computational methods section, the calculated frequency shifts based on the nitrile Stark response and the field at the nitrile nitrogen are plotted against the charge density of anions in Figure 5a. Consistent with experimental results, a red shift with respect to increasing charge density is observed. Frequency shifts based on electric field values at the nitrile carbon atom are included in SI Figure S6a and show a similar trend. While the trend in experimental data is reproduced computationally, the magnitude of the computed frequency shifts is larger than experimentally observed ones. The possible origins of this will be discussed in the discussion section.

One may argue that the observed trend is not necessarily a consequence of ionic size, but rather majorly their structural and chemical details. To gain insight into this issue, we constructed a simplified model, in which only the size of the anion was varied, without affecting their shape. Model systems were constructed by starting from a Cl^- anion and

modifying its Lennard-Jones σ parameter, while keeping all other force field parameters the same. This gives rise to various Cl^- anions with artificially enlarged volumes. We use 1.5, 2, and 3 times the original value of σ (4.04 Å) to construct the IL systems, named $[EMIM]^+[Cl_{1.5\sigma}]^-$, $[EMIM]^+[Cl_{2\sigma}]^-$, and $[EMIM]^+[Cl_{3\sigma}]^-$ respectively. The effective radii of the anions are, therefore scaled by a factor of 1.5, 2, and 3 while maintaining the spherical shape. MD simulations are performed for this anion series, while the cation is still kept to be $[EMIM]^+$. The frequency shifts of the probe molecule, based on field at the nitrogen of nitrile, are plotted against the relative charge density of this chloride series, calculated using the ratio of ionic radii (Figure 5b). The figure shows that the trend with respect to size indeed holds when only the size of the anion is changed. The origin of this change with respect to ion size will be discussed in discussion section. Frequency shifts for the chloride series calculated based on the field on the carbon atoms of nitrile are included in the SI (Figure S6b) and show a similar behavior.

Figure 6 shows snapshots of representative systems at the end of production runs. Inspection of these snapshots for the experimental anion series (left panel) and the model chloride series (right panel) reveal the relative positions of cations and anions at the interface. We note that for anion series used in the experiments, the closest layer to the 4-MBN ligands is predominantly made of anions. Moreover, the anions show different degrees of intercalation into the 4-MBN layer. Smaller anions such as Br^- and Cl^- fully insert themselves into the 4-MBN layer and lie in the same plane as the nitrile nitrogens. Larger $[BF_4]^-$ anions show partial insertions, and even larger $[FAP]^-$ anions cannot intercalate and are excluded from the monolayer. The density of anions at the interface is also less for larger anions, as expected. A similar behavior is observed for the model chloride series (Figure 6, right panel). The normal size chloride intercalates into the monolayer, while the largest model chloride is excluded from the surface. The ionic density near the surface is also the smallest for the largest of the chloride series anion.

To rationalize the frequency shift-size trends, we calculated the symmetrized number

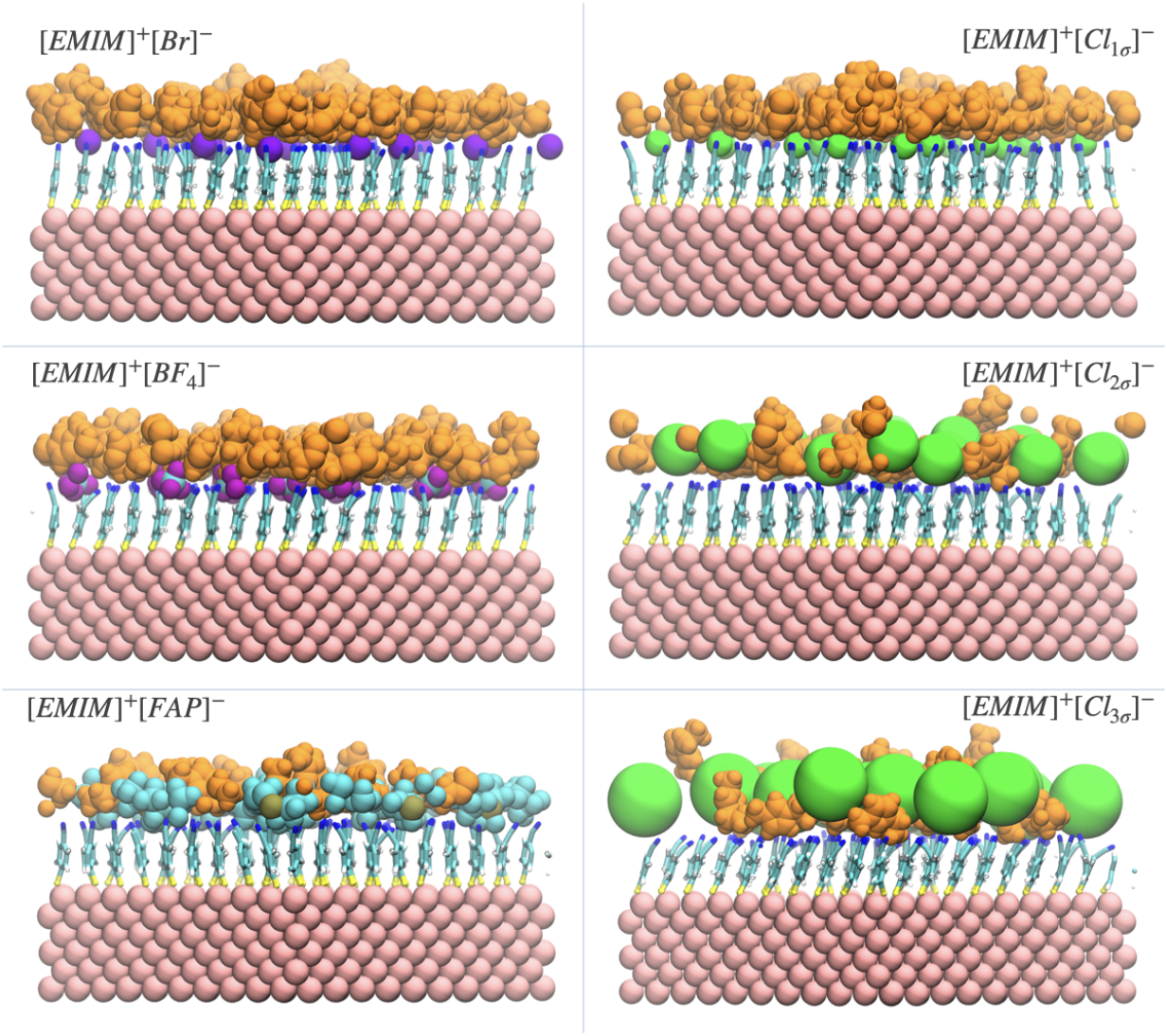

Figure 6: Snapshots of representative systems after 200 ns of production MD. Only top half of the functionalized gold slab has been shown. For realistic anions, full IL residues have been shown for atoms within 4 Å of nitrile nitrogens. For $[EMIM]^+[Cl_{2\sigma}]^-$ and $[EMIM]^+[Cl_{3\sigma}]^-$, the selection thresholds are 6 Å and 8 Å respectively.

density of a few representative atoms (see Scheme 1 for special atom names). Figure 7 shows the distribution of these atoms along the box's positive z-axis, centered around the gold slab. Symmetrized number densities and charge densities of all realistic and model systems are included in the SI (Figure S7a,S7b,S8a,S8b). We should note that the density profiles are of unique atoms in IL residues, they are not cumulative of any atom type (such as F_P in $[FAP]^-$). The position distributions of nitrile nitrogen atoms have been shaded green for reference. The overlap of the black lines (representing key anionic atoms such as Br, F, F_P, and Cl) with green region depicts the extent of anionic intercalation into the 4-MBN layer. Number density of three key imidazole hydrogens (see Scheme 1) from $[EMIM]^+$ cations have also been shown in the figure. The hydrogen with highest partial charge (H3) is shown in red; whereas the other two (H4, H5) have been shown in orange. Higher density of one type of hydrogen over others, as seen in $[EMIM]^+[Br]^-$, $[EMIM]^+[Cl]^+$, and $[EMIM]^+[BF_4]^-$ indicate preferential orientation of cations near the interface.

Discussion

The main objective of this study is to understand the organization of ILs near the interface by measuring the frequency shift of the probe molecule adsorbed on the metal. Our results show a systematic change in the vibrational frequency of the probe with increasing anion size. However, this information alone cannot provide a complete molecular picture of the local ionic structure, since ordering of ions of varying sizes is complex and not uniquely associated with a single value of frequency shift. Therefore, we complemented the experimental work with MD simulations with two purposes - first to find out whether the experimental trends were reproduced by the simulations, and second to identify the underlying structural origins of the observed trends.

The primary takeaway from these combined efforts is that IL molecular structure at the interface is dictated by the ability of ions to pack and organize near the surface. The most

important result from MD simulations is the tendency for the anions to partially intercalate within the SAM. The smallest anion (bromide) readily fits between the 4-MBN molecules and intercalates into the monolayer, residing at the same depth as the nitrogen atoms of the nitrile (Figure 7). This insertion, in turn, supports a high packing density of $EMIM^+$ in the next layer. The large interfacial charge density strongly polarizes the SAM, resulting in a considerable shift in the nitrile frequency. However, as the size of the anions in the IL is increased, their ability to insert within the SAM is diminished. Furthermore, the large anion sizes exclude some volume near the surface and push the cation-dominated layer away from the SAM. This results in low density of the cations and larger distance between the cations and the monolayer. Therefore, a smaller field is experienced by the probe, leading to smaller frequency shifts.

The above scenario even holds to explain the slightly out-of-order behavior of acetate in $[EMIM]^+[AcO]^-$, which is observed experimentally (Figures 3,4) and confirmed computationally (Figure S7a,S7b). In both cases, the acetate anion causes a frequency shift in the probe that is larger than anticipated from its effective size, appearing in both the experimental and computational results as a slight non-monotonic deviation from the trend. In this case, the molecular shape of the acetate together with the intercalation description given above explains this effect. The charged portion of the acetate ion (delocalized mainly over the oxygens) is relatively compact and available for insertion in the monolayer. Similar to the behavior of $[EMIM]^+[Br]^-$ or $[EMIM]^+[Cl]^-$, this insertion supports the formation of a high-density layer of $[EMIM]^+$ cations near the SAM and the resulting structure polarizes the nitrile more than anticipated based on the total net size of the acetate.

The use of the chloride model system is a way to investigate the fundamental dependence of interfacial solvation on anion size without the confounding effects of molecular structure. The results from these simulations show a similar overall trend but the calculated fields depend monotonically on anion size, thereby confirming the hypothesis that insertion and packing is at the core of this behavior. We observe the same ion intercalation structure in

the model chloride system as the atomistic anions (Figure 6 and 7). The center of anionic charge is pushed away from the interface as the anion size increases. However, at the limit of chlorides with large values of σ, the first ionic layer becomes predominantly cationic, which we do not observe for ILs like $[EMIM]^+[FAP]^-$. In both cases, the packing density and the induced field are small, therefore confirming that packing density may be a stronger factor in dictating the interfacial field compared to solely relying on the ordering of the layers.

We note that some parts of the larger anions (e.g. the fluorines in $[FAP]^-$) also penetrate the 4-MBN layer to a similar extent (Figure 7) as Br^-. However, a second fluorine peak is observed for both $[EMIM]^+[BF_4]^-$ and $[EMIM]^+[FAP]^-$ oustide the monolayer, indicating that large anions are only partially interecalated in the monolayer and mainly reside outside. This behavior is also observed for $[EMIM]^+[DMP]^-$ as seen in the SI. Due to this effect, and the larger sizes of these anions, the overall charge density near the surface is much smaller compared to $[EMIM]^+[Br]^-$, thereby producing a smaller field experienced by the probe molecule.

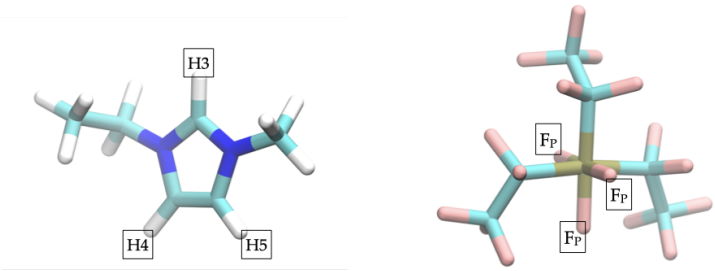

Scheme 1

Though the overall trend between interfacial fields and anion size holds between theory and experiment, the computed fields exceed the measured fields for every IL we studied. This discrepancy is the greatest for larger anions (factor of ~ 7 for $[FAP]^-$). We hypothesize that this is a limitation of the fixed-charge non-polarizable nature of our force field. Inclusion of polarizable force fields will modify metal-ion and ion-ion interactions and may result in an overall decrease in the calculated interfacial fields. Furthermore, the location

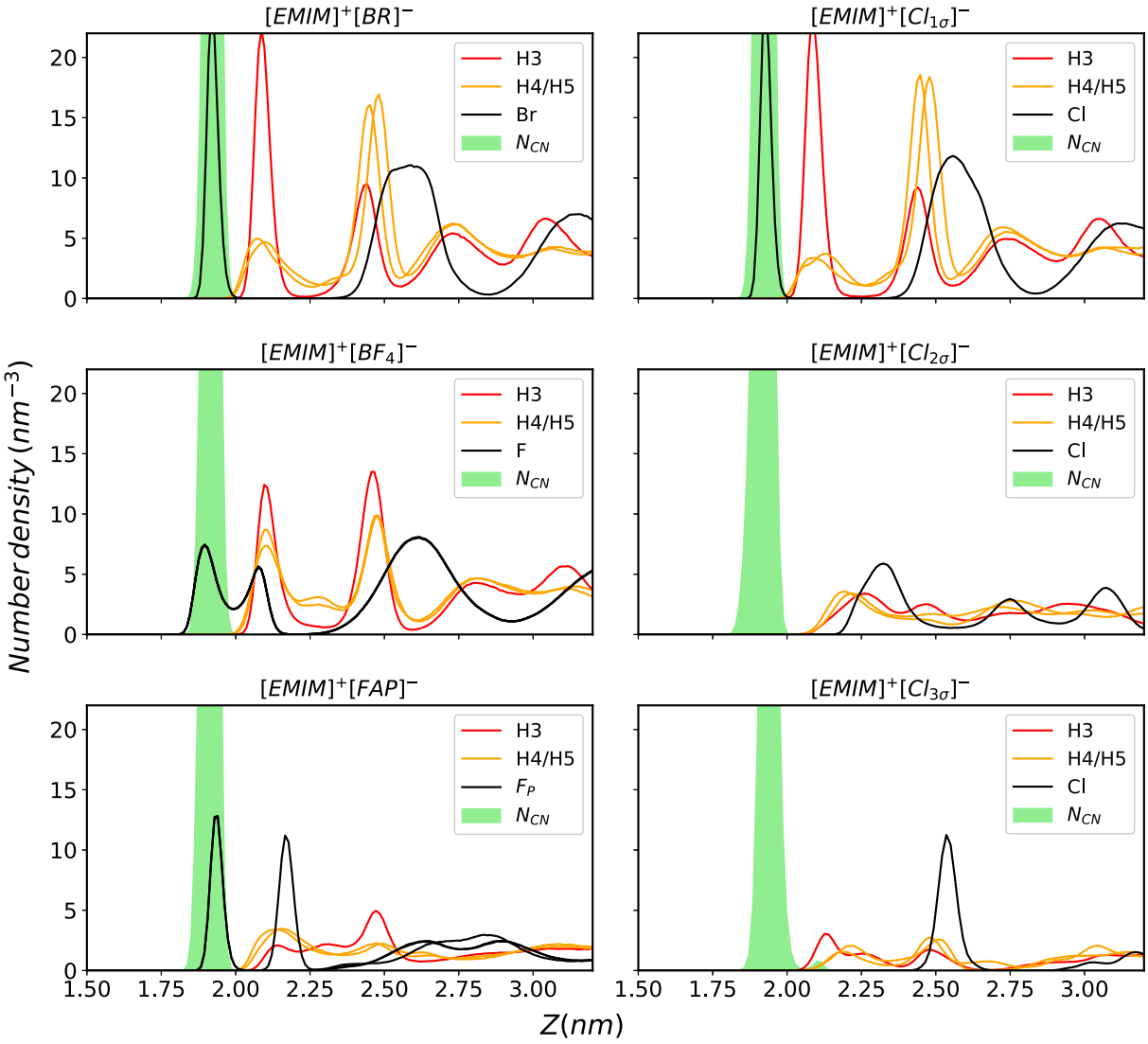

Figure 7: Symmetrized partial number density of representative atoms plotted against average relative position from the center of gold layer. As a reference, the positions of nitrile nitrogen (N_{CN}) atoms of 4-MBN monolayer are shown in green. $[EMIM]^+$ hydrogens from imidazole ring are labelled as H3 (H atom at 3^{rd} position of imidazole ring), H4 and H5. All four F atoms of $[BF_4]^-$ anions are labelled F. The F atoms directly attached to phosphorus center in $[FAP]^-$ are labelled F_P. The atom names for larger ions are illustrated in Scheme 1.

at which field values are calculated is chosen at a single point within the probe molecule. Our previous work shows that fields near interfaces are not uniform, and vary across the length of the probe molecule.[115] Therefore, choosing a single point within the molecule only approximately emulates the homogeneous field Stark effect. For the purposes of this study, which is identifying the size effects trends, this does not pose any problems.

A comment related to the water content of ILs is necessary for our work. As many previous work have shown, ILs are hygroscopic and water adsorbed from the atmosphere alters their properties in important ways. The partition of water between interface and bulk in ILs probed by a 4-MBN SAM was reported by us recently.[116] Based on that work, even though ILs adsorb water readily, if the quantity of the water is small it is favorably solvated within the bulk and it hardly appears at the interface. A significantly large critical threshold (above ~ 0.8 mole fraction) must be reached before water has a significant partition at the surface. As discussed in the experimental section, we have taken steps to dry the ILs studied in this work and therefore the water content should be minimal. Based on the results from our previous study, the measurements reported in this work are representative of water-free ILs.

Further characterization of IL-metal interfaces using this joint experimental-computational approach could include the measurement and simulation of charged interfaces along a similar series of ion structure. We have used VSFG to probe the electrified metal-IL interface,[20] but that previous work did not cover systematic variation of ion composition. Modifying particular chemical properties of ILs (such as introducing hydrophobic moieties) will also provide fundamental information about ionic structure at the interface.

Concluding remarks

In this study, we take a detailed look at the structure and electrostatics of ILs near a metal interface functionalized by a layer of probe molecules. The main takeaway form our work is

that the local electric field sensed by the probes varies significantly with the size of the anions in the imidazolium family of ILs, with larger anions producing smaller interfacial fields. The origin of this effect was revealed by our molecular dynamics simulations. We observe that small anions intercalate into the nitrile probe layer which helps with tighter packing of the nearby cation layer and results in large electric fields. As the size of the anions increase, the extent of surface penetration diminishes, leading to disappearance of the ordered structure and looser packing of ions near the surface. We also emphasize that not only size, but also the shape of the anions is important in dictating the local electric field. Finally, the trends in calculated Stark frequency shifts qualitatively agree with experiments. This work is a stepping stone towards understanding and modifying interfacial fields in the presence of complex ionic environments.

Acknowledgement

The authors gratefully acknowledge support from several sources. SS and JD were supported by the Air Force Office of Scientific Research AFOSR award FA9550-18-1-0021. JP and JD were supported by the NSF CAREER Award (1454467). MV and AP were supported by Air Force Office of Scientific Research AFOSR award FA9550-18-1-0420. The computational component was supported by a grant from the National Science Foundation to QC (CHE-1829555). Computational resources from the Extreme Science and Engineering Discovery Environment (XSEDE), which is supported by NSF grant number OCI-1053575, are greatly appreciated; part of the computational work was performed on the Shared Computing Cluster which is administered by Boston University's Research Computing Services (URL: www.bu.edu/tech/support/research/).

Supporting Information Available

The supplementary information has further plots, tables and commentary relevant to the main text.

References

(1) Patel, D. D.; Lee, J.-M. Applications of ionic liquids. *The Chemical Record* **2012**, *12*, 329–355.

(2) Plechkova, N. V.; Seddon, K. R. Applications of ionic liquids in the chemical industry. *Chemical Society Reviews* **2008**, *37*, 123–150.

(3) Ohno, H. *Electrochemical aspects of ionic liquids*; John Wiley & Sons, 2011.

(4) Zhang, Q.; Shreeve, J. M. Ionic liquid propellants: Future fuels for space propulsion. *Chemistry–A European Journal* **2013**, *19*, 15446–15451.

(5) Fedorov, M. V.; Kornyshev, A. A. Ionic liquids at electrified interfaces. *Chemical reviews* **2014**, *114*, 2978–3036.

(6) Reichert, P.; Kjær, K. S.; van Driel, T. B.; Mars, J.; Ochsmann, J. W.; Pontoni, D.; Deutsch, M.; Nielsen, M. M.; Mezger, M. Molecular scale structure and dynamics at an ionic liquid/electrode interface. *Faraday discussions* **2017**, *206*, 141–157.

(7) Tokuda, H.; Hayamizu, K.; Ishii, K.; Susan, M. A. B. H.; Watanabe, M. Physicochemical properties and structures of room temperature ionic liquids. 1. Variation of anionic species. *The Journal of Physical Chemistry B* **2004**, *108*, 16593–16600.

(8) Levin, Y. Electrostatic correlations: from plasma to biology. *Reports on progress in physics* **2002**, *65*, 1577.

(9) Rosenfeld, Y. Free energy model for inhomogeneous fluid mixtures: Yukawa-charged hard spheres, general interactions, and plasmas. *The Journal of chemical physics* **1993**, *98*, 8126–8148.

(10) Freyland, W. *Coulombic fluids: bulk and interfaces*; Springer Science & Business Media, 2011; Vol. 168.

(11) Lynden-Bell, R. M.; Frolov, A.; Fedorov, M. V. Electrode screening by ionic liquids. *Physical Chemistry Chemical Physics* **2012**, *14*, 2693–2701.

(12) Nishi, N.; Uchiyashiki, J.; Ikeda, Y.; Katakura, S.; Oda, T.; Hino, M.; Yamada, N. L. Potential-dependent structure of the ionic layer at the electrode interface of an ionic liquid probed using neutron reflectometry. *The Journal of Physical Chemistry C* **2019**, *123*, 9223–9230.

(13) Watanabe, S.; Pilkington, G. A.; Oleshkevych, A.; Pedraz, P.; Radiom, M.; Welbourn, R.; Glavatskih, S.; Rutland, M. W. Interfacial structuring of non-halogenated imidazolium ionic liquids at charged surfaces: effect of alkyl chain length. *Physical Chemistry Chemical Physics* **2020**, *22*, 8450–8460.

(14) Ratti, R. Ionic Liquids: Synthesis and Applications in Catalysis. *Advances in Chemistry* **2014**, *2014*.

(15) Taylor, A. W.; Licence, P.; Abbott, A. P. Non-classical diffusion in ionic liquids. *Physical Chemistry Chemical Physics* **2011**, *13*, 10147–10154.

(16) Wang, H.; Pilon, L. Intrinsic limitations of impedance measurements in determining electric double layer capacitances. *Electrochimica Acta* **2012**, *63*, 55–63.

(17) Gnahm, M.; Pajkossy, T.; Kolb, D. The interface between Au (111) and an ionic liquid. *Electrochimica Acta* **2010**, *55*, 6212–6217.

(18) Drüschler, M.; Roling, B. Commentary on 'The interface between Au (111) and an ionic liquid'. *Electrochimica Acta* **2011**, *56*, 7243–7245.

(19) Roling, B.; Drüschler, M. Comments on "Intrinsic limitations of impedance measurements in determining electric double layer capacitances" by H. Wang and L. Pilon [Electrochim. Acta 63 (2012) 55]. *Electrochimica Acta* **2012**, *76*, 526–528.

(20) Sarkar, S.; Patrow, J. G.; Voegtle, M. J.; Pennathur, A. K.; Dawlaty, J. M. Electrodes as Polarizing Functional Groups: Correlation between Hammett Parameters and Electrochemical Polarization. *The Journal of Physical Chemistry C* **2019**, *123*, 4926–4937.

(21) Patrow, J. G.; Sorenson, S. A.; Dawlaty, J. M. Direct spectroscopic measurement of interfacial electric fields near an electrode under polarizing or current-carrying conditions. *The Journal of Physical Chemistry C* **2017**, *121*, 11585–11592.

(22) Staffa, J. K.; Lorenz, L.; Stolarski, M.; Murgida, D. H.; Zebger, I.; Utesch, T.; Kozuch, J.; Hildebrandt, P. Determination of the local electric field at Au/SAM interfaces using the vibrational Stark effect. *The Journal of Physical Chemistry C* **2017**, *121*, 22274–22285.

(23) Sorenson, S. A.; Patrow, J. G.; Dawlaty, J. M. Solvation reaction field at the interface measured by vibrational sum frequency generation spectroscopy. *Journal of the American Chemical Society* **2017**, *139*, 2369–2378.

(24) Patrow, J. G.; Wang, Y.; Dawlaty, J. M. Interfacial Lewis Acid–Base Adduct Formation Probed by Vibrational Spectroscopy. *The journal of physical chemistry letters* **2018**, *9*, 3631–3638.

(25) Lewis, N. H.; Iscen, A.; Felts, A.; Dereka, B.; Schatz, G. C.; Tokmakoff, A. Vibrational Probe of Aqueous Electrolytes: The Field Is Not Enough. *The Journal of Physical Chemistry B* **2020**, *124*, 7013–7026.

(26) Goldsmith, Z. K.; Secor, M.; Hammes-Schiffer, S. Inhomogeneity of Interfacial Electric Fields at Vibrational Probes on Electrode Surfaces. *ACS central science* **2020**, *6*, 304–311.

(27) Lynden-Bell, R. Gas—liquid interfaces of room temperature ionic liquids. *Molecular Physics* **2003**, *101*, 2625–2633.

(28) Lynden-Bell, R.; Del Popolo, M. Simulation of the surface structure of butylmethylimidazolium ionic liquids. *Physical Chemistry Chemical Physics* **2006**, *8*, 949–954.

(29) Sloutskin, E.; Lynden-Bell, R.; Balasubramanian, S.; Deutsch, M. The surface structure of ionic liquids: Comparing simulations with x-ray measurements. *The Journal of chemical physics* **2006**, *125*, 174715.

(30) Yan, T.; Li, S.; Jiang, W.; Gao, X.; Xiang, B.; Voth, G. A. Structure of the liquid-vacuum interface of room-temperature ionic liquids: A molecular dynamics study. *The Journal of Physical Chemistry B* **2006**, *110*, 1800–1806.

(31) Pinilla, C.; Del Popolo, M. G.; Lynden-Bell, R. M.; Kohanoff, J. Structure and dynamics of a confined ionic liquid. Topics of relevance to dye-sensitized solar cells. *The Journal of Physical Chemistry B* **2005**, *109*, 17922–17927.

(32) Pinilla, C.; Del Pópolo, M.; Kohanoff, J.; Lynden-Bell, R. Polarization relaxation in an ionic liquid confined between electrified walls. *The Journal of Physical Chemistry B* **2007**, *111*, 4877–4884.

(33) Kislenko, S. A.; Samoylov, I. S.; Amirov, R. H. Molecular dynamics simulation of the electrochemical interface between a graphite surface and the ionic liquid [BMIM][PF 6]. *Physical Chemistry Chemical Physics* **2009**, *11*, 5584–5590.

(34) Ntim, S.; Sulpizi, M. Role of image charges in ionic liquid confined between metallic interfaces. *Physical Chemistry Chemical Physics* **2020**, *22*, 10786–10791.

(35) Zhang, S.; Zhang, Y.; Ma, X.; Lu, L.; He, Y.; Deng, Y. Benzonitrile as a probe of local environment in ionic liquids. *The Journal of Physical Chemistry B* **2013**, *117*, 2764–2772.

(36) Peñalber, C. Y.; Baker, G. A.; Baldelli, S. Sum frequency generation spectroscopy of imidazolium-based ionic liquids with cyano-functionalized anions at the solid salt–liquid interface. *The Journal of Physical Chemistry B* **2013**, *117*, 5939–5949.

(37) Rivera-Rubero, S.; Baldelli, S. Surface characterization of 1-butyl-3-methylimidazolium Br-, I-, PF6-, BF4-,(CF3SO2) 2N-, SCN-, CH3SO3-, CH3SO4-, and (CN) 2N-ionic liquids by sum frequency generation. *The Journal of Physical Chemistry B* **2006**, *110*, 4756–4765.

(38) Baldelli, S. Surface structure at the ionic liquid- electrified metal interface. *Accounts of chemical research* **2008**, *41*, 421–431.

(39) Rivera-Rubero, S.; Baldelli, S. Influence of water on the surface of hydrophilic and hydrophobic room-temperature ionic liquids. *Journal of the American Chemical Society* **2004**, *126*, 11788–11789.

(40) García, N.; Dlott, D. Vibrational Sum Frequency Study of the Influence of Water-Ionic Liquid Mixtures in the CO2 Electroreduction on Silver Electrodes. 70th International Symposium on Molecular Spectroscopy: June 22-26, 2015 at The University of Illinois at Urbana-Champaign. Talk FB05. 2015.

(41) García Rey, N.; Dlott, D. D. Structural Transition in an Ionic Liquid Controls CO2 Electrochemical Reduction. *The Journal of Physical Chemistry C* **2015**, *119*, 20892–20899.

(42) Rosen, B. A.; Haan, J. L.; Mukherjee, P.; Braunschweig, B.; Zhu, W.; Salehi-Khojin, A.; Dlott, D. D.; Masel, R. I. In situ spectroscopic examination of a low

overpotential pathway for carbon dioxide conversion to carbon monoxide. *The Journal of Physical Chemistry C* **2012**, *116*, 15307–15312.

(43) Tamimi, A.; Bailey, H. E.; Fayer, M. D. Alkyl Chain Length Dependence of the Dynamics and Structure in the Ionic Regions of Room-Temperature Ionic Liquids. *The Journal of Physical Chemistry B* **2016**, *120*, 7488–7501.

(44) Giammanco, C. H.; Kramer, P. L.; Yamada, S. A.; Nishida, J.; Tamimi, A.; Fayer, M. D. Carbon dioxide in an ionic liquid: Structural and rotational dynamics. *The Journal of chemical physics* **2016**, *144*, 104506.

(45) Fayer, M. D. Dynamics and structure of room temperature ionic liquids. *Chemical Physics Letters* **2014**, *616*, 259–274.

(46) Humbert, C.; Busson, B.; Six, C.; Gayral, A.; Gruselle, M.; Villain, F.; Tadjeddine, A. Sum-Frequency Generation as a Vibrational and Electronic Probe of The Electrochemical Interface and Thin Films. *J. Electroanal. Chem.* **2008**, *621*, 314–321.

(47) Shalhout, F. Y.; Malyk, S.; Benderskii, A. V. Relative phase change of nearby resonances in temporally delayed sum frequency spectra. *The journal of physical chemistry letters* **2012**, *3*, 3493–3497.

(48) Wijesuriya, S.; Burugapalli, K.; Mackay, R.; Ajaezi, G.; Balachandran, W. Chemically roughened solid silver: A simple, robust and broadband SERS substrate. *Sensors* **2016**, *16*, 1742.

(49) Ha, S. H.; Mai, N. L.; Koo, Y.-M. Microwave-assisted separation of ionic liquids from aqueous solution of ionic liquids. *Journal of Chromatography A* **2010**, *1217*, 7638–7641.

(50) Jo, S.; Kim, T.; Iyer, V. G.; Im, W. CHARMM-GUI: a web-based graphical user interface for CHARMM. *Journal of computational chemistry* **2008**, *29*, 1859–1865.

(51) Brooks, B. R.; Brooks III, C. L.; Mackerell Jr, A. D.; Nilsson, L.; Petrella, R. J.; Roux, B.; Won, Y.; Archontis, G.; Bartels, C.; Boresch, S. e. a. CHARMM: the biomolecular simulation program. *Journal of computational chemistry* **2009**, *30*, 1545–1614.

(52) Hansen, J.-P.; McDonald, I. R. *Theory of simple liquids*; Elsevier, 1990.

(53) Margulis, C.; Stern, H.; Berne, B. Computer simulation of a "green chemistry" room-temperature ionic solvent. *The Journal of Physical Chemistry B* **2002**, *106*, 12017–12021.

(54) Morrow, T. I.; Maginn, E. J. Molecular dynamics study of the ionic liquid 1-n-butyl-3-methylimidazolium hexafluorophosphate. *The Journal of Physical Chemistry B* **2002**, *106*, 12807–12813.

(55) Del Pópolo, M. G.; Voth, G. A. On the structure and dynamics of ionic liquids. *The Journal of Physical Chemistry B* **2004**, *108*, 1744–1752.

(56) Yan, T.; Burnham, C. J.; Del Pópolo, M. G.; Voth, G. A. Molecular dynamics simulation of ionic liquids: The effect of electronic polarizability. *The Journal of Physical Chemistry B* **2004**, *108*, 11877–11881.

(57) McDaniel, J. G.; Yethiraj, A. Influence of electronic polarization on the structure of ionic liquids. *The journal of physical chemistry letters* **2018**, *9*, 4765–4770.

(58) Bedrov, D.; Borodin, O.; Li, Z.; Smith, G. D. Influence of polarization on structural, thermodynamic, and dynamic properties of ionic liquids obtained from molecular dynamics simulations. *The Journal of Physical Chemistry B* **2010**, *114*, 4984–4997.

(59) Fujii, K.; Soejima, Y.; Kyoshoin, Y.; Fukuda, S.; Kanzaki, R.; Umebayashi, Y.; Yamaguchi, T.; Ishiguro, S.-i.; Takamuku, T. Liquid structure of room-temperature ionic

liquid, 1-ethyl-3-methylimidazolium bis-(trifluoromethanesulfonyl) imide. *The Journal of Physical Chemistry B* **2008**, *112*, 4329–4336.

(60) Canongia Lopes, J. N.; Deschamps, J.; Pádua, A. A. Modeling ionic liquids using a systematic all-atom force field. *The Journal of Physical Chemistry B* **2004**, *108*, 2038–2047.

(61) MacKerell Jr, A. D.; Bashford, D.; Bellott, M.; Dunbrack Jr, R. L.; Evanseck, J. D.; Field, M. J.; Fischer, S.; Gao, J.; Guo, H.; Ha, S. e. a. All-atom empirical potential for molecular modeling and dynamics studies of proteins. *The journal of physical chemistry B* **1998**, *102*, 3586–3616.

(62) Huang, J.; MacKerell Jr, A. D. CHARMM36 all-atom additive protein force field: Validation based on comparison to NMR data. *Journal of computational chemistry* **2013**, *34*, 2135–2145.

(63) Vanommeslaeghe, K.; Hatcher, E.; Acharya, C.; Kundu, S.; Zhong, S.; Shim, J.; Darian, E.; Guvench, O.; Lopes, P.; Vorobyov, I. e. a. CHARMM general force field: A force field for drug-like molecules compatible with the CHARMM all-atom additive biological force fields. *Journal of computational chemistry* **2010**, *31*, 671–690.

(64) Vanommeslaeghe, K.; MacKerell Jr, A. D. Automation of the CHARMM General Force Field (CGenFF) I: bond perception and atom typing. *Journal of chemical information and modeling* **2012**, *52*, 3144–3154.

(65) Vanommeslaeghe, K.; Raman, E. P.; MacKerell Jr, A. D. Automation of the CHARMM General Force Field (CGenFF) II: assignment of bonded parameters and partial atomic charges. *Journal of chemical information and modeling* **2012**, *52*, 3155–3168.

(66) Yu, W.; He, X.; Vanommeslaeghe, K.; MacKerell Jr, A. D. Extension of the CHARMM

general force field to sulfonyl-containing compounds and its utility in biomolecular simulations. *Journal of computational chemistry* **2012**, *33*, 2451–2468.

(67) Canongia Lopes, J. N.; Pádua, A. A. Molecular force field for ionic liquids III: Imidazolium, pyridinium, and phosphonium cations; chloride, bromide, and dicyanamide anions. *The Journal of Physical Chemistry B* **2006**, *110*, 19586–19592.

(68) Perdew, J. P.; Chevary, J. A.; Vosko, S. H.; Jackson, K. A.; Pederson, M. R.; Singh, D. J.; Fiolhais, C. Atoms, molecules, solids, and surfaces: Applications of the generalized gradient approximation for exchange and correlation. *Physical review B* **1992**, *46*, 6671.

(69) Perdew, J. P.; Chevary, J.; Vosko, S.; Jackson, K. A.; Pederson, M. R.; Singh, D.; Fiolhais, C. Erratum: Atoms, molecules, solids, and surfaces: Applications of the generalized gradient approximation for exchange and correlation. *Physical Review B* **1993**, *48*, 4978.

(70) Perdew, J. P.; Burke, K.; Wang, Y. Generalized gradient approximation for the exchange-correlation hole of a many-electron system. *Phys. Rev. B* **1996**, *54*, 16533–16539.

(71) Miehlich, B.; Savin, A.; Stoll, H.; Preuss, H. Results obtained with the correlation energy density functionals of becke and Lee, Yang and Parr. *Chemical Physics Letters* **1989**, *157*, 200 – 206.

(72) Lee, C.; Yang, W.; Parr, R. G. Development of the Colle-Salvetti correlation-energy formula into a functional of the electron density. *Phys. Rev. B* **1988**, *37*, 785–789.

(73) Becke, A. D. Density-functional exchange-energy approximation with correct asymptotic behavior. *Phys. Rev. A* **1988**, *38*, 3098–3100.

(74) Wilson, A. K.; van Mourik, T.; Dunning Jr, T. H. Gaussian basis sets for use in correlated molecular calculations. VI. Sextuple zeta correlation consistent basis sets for boron through neon. *Journal of Molecular Structure: THEOCHEM* **1996**, *388*, 339–349.

(75) Frisch, M. J.; Trucks, G. W.; Schlegel, H. B.; Scuseria, G. E.; Robb, M. A.; Cheeseman, J. R.; Scalmani, G.; Barone, V.; Petersson, G. A.; Nakatsuji, H. et al. Gaussian˜16 Revision C.01. 2016; Gaussian Inc. Wallingford CT.

(76) de Andrade, J.; Böes, E. S.; Stassen, H. Computational study of room temperature molten salts composed by 1-alkyl-3-methylimidazolium cations force-field proposal and validation. *The journal of physical chemistry B* **2002**, *106*, 13344–13351.

(77) Fox, T.; Kollman, P. A. Application of the RESP methodology in the parametrization of organic solvents. *The Journal of Physical Chemistry B* **1998**, *102*, 8070–8079.

(78) Gough, C. A.; Debolt, S. E.; Kollman, P. A. Derivation of fluorine and hydrogen atom parameters using liquid simulations. *Journal of computational chemistry* **1992**, *13*, 963–970.

(79) Mayo, S. L.; Olafson, B. D.; Goddard, W. A. DREIDING: a generic force field for molecular simulations. *Journal of Physical chemistry* **1990**, *94*, 8897–8909.

(80) Kim, S.; Lee, J.; Jo, S.; Brooks III, C. L.; Lee, H. S.; Im, W. CHARMM-GUI ligand reader and modeler for CHARMM force field generation of small molecules. *Journal of Computational Chemistry* **2017**, *38*, 1879–1886.

(81) Shimizu, K.; Almantariotis, D.; Gomes, M. F. C.; Padua, A. A.; Canongia Lopes, J. N. Molecular force field for ionic liquids V: Hydroxyethylimidazolium, dimethoxy-2-methylimidazolium, and fluoroalkylimidazolium cations and bis (fluorosulfonyl) amide, perfluoroalkanesulfonylamide, and fluoroalkylfluorophosphate anions. *The Journal of Physical Chemistry B* **2010**, *114*, 3592–3600.

(82) Noda, A.; Hayamizu, K.; Watanabe, M. Pulsed-gradient spin- echo 1H and 19F NMR ionic diffusion coefficient, viscosity, and ionic conductivity of non-chloroaluminate room-temperature ionic liquids. *The Journal of Physical Chemistry B* **2001**, *105*, 4603–4610.

(83) Every, H. A.; Bishop, A. G.; MacFarlane, D. R.; Orädd, G.; Forsyth, M. Transport properties in a family of dialkylimidazolium ionic liquids. *Physical chemistry chemical physics* **2004**, *6*, 1758–1765.

(84) Urahata, S. M.; Ribeiro, M. C. Single particle dynamics in ionic liquids of 1-alkyl-3-methylimidazolium cations. *The Journal of chemical physics* **2005**, *122*, 024511.

(85) Rey-Castro, C.; Tormo, A.; Vega, L. F. Effect of the flexibility and the anion in the structural and transport properties of ethyl-methyl-imidazolium ionic liquids. *Fluid phase equilibria* **2007**, *256*, 62–69.

(86) Rey-Castro, C.; Vega, L. F. Transport properties of the ionic liquid 1-ethyl-3-methylimidazolium chloride from equilibrium molecular dynamics simulation. The effect of temperature. *The Journal of Physical Chemistry B* **2006**, *110*, 14426–14435.

(87) Kowsari, M.; Alavi, S.; Ashrafizaadeh, M.; Najafi, B. Molecular dynamics simulation of imidazolium-based ionic liquids. I. Dynamics and diffusion coefficient. *The Journal of chemical physics* **2008**, *129*, 224508.

(88) Heinz, H.; Vaia, R.; Farmer, B.; Naik, R. Accurate simulation of surfaces and interfaces of face-centered cubic metals using 12- 6 and 9- 6 Lennard-Jones potentials. *The Journal of Physical Chemistry C* **2008**, *112*, 17281–17290.

(89) Heinz, H.; Lin, T.-J.; Kishore Mishra, R.; Emami, F. S. Thermodynamically consistent force fields for the assembly of inorganic, organic, and biological nanostructures: the INTERFACE force field. *Langmuir* **2013**, *29*, 1754–1765.

(90) Abraham, M. J.; Murtola, T.; Schulz, R.; Páll, S.; Smith, J. C.; Hess, B.; Lindahl, E. GROMACS: High performance molecular simulations through multi-level parallelism from laptops to supercomputers. *SoftwareX* **2015**, *1*, 19–25.

(91) Páll, S.; Abraham, M. J.; Kutzner, C.; Hess, B.; Lindahl, E. Tackling exascale software challenges in molecular dynamics simulations with GROMACS. International conference on exascale applications and software. 2014; pp 3–27.

(92) Pronk, S.; Páll, S.; Schulz, R.; Larsson, P.; Bjelkmar, P.; Apostolov, R.; Shirts, M. R.; Smith, J. C.; Kasson, P. M.; van der Spoel, D. e. a. GROMACS 4.5: a high-throughput and highly parallel open source molecular simulation toolkit. *Bioinformatics* **2013**, *29*, 845–854.

(93) Hess, B.; Kutzner, C.; Van Der Spoel, D.; Lindahl, E. GROMACS 4: algorithms for highly efficient, load-balanced, and scalable molecular simulation. *Journal of chemical theory and computation* **2008**, *4*, 435–447.

(94) Van Der Spoel, D.; Lindahl, E.; Hess, B.; Groenhof, G.; Mark, A. E.; Berendsen, H. J. GROMACS: fast, flexible, and free. *Journal of computational chemistry* **2005**, *26*, 1701–1718.

(95) Lindahl, E.; Hess, B.; Van Der Spoel, D. GROMACS 3.0: a package for molecular simulation and trajectory analysis. *Molecular modeling annual* **2001**, *7*, 306–317.

(96) Berendsen, H. J.; van der Spoel, D.; van Drunen, R. GROMACS: a message-passing parallel molecular dynamics implementation. *Computer physics communications* **1995**, *91*, 43–56.

(97) mesh Ewald, P. An N.log (N) method for Ewald sums in large systems. *J. Chem. Phys* **1993**, *98*, 10089–10092.

(98) Hess, B.; Bekker, H.; Berendsen, H. J.; Fraaije, J. G. LINCS: a linear constraint solver for molecular simulations. *Journal of computational chemistry* **1997**, *18*, 1463–1472.

(99) Hess, B. P-LINCS: A parallel linear constraint solver for molecular simulation. *Journal of chemical theory and computation* **2008**, *4*, 116–122.

(100) Berendsen, H. J.; Postma, J. v.; van Gunsteren, W. F.; DiNola, A.; Haak, J. R. Molecular dynamics with coupling to an external bath. *The Journal of chemical physics* **1984**, *81*, 3684–3690.

(101) Nosé, S. A molecular dynamics method for simulations in the canonical ensemble. *Molecular physics* **1984**, *52*, 255–268.

(102) Hoover, W. G. Canonical dynamics: Equilibrium phase-space distributions. *Physical review A* **1985**, *31*, 1695.

(103) Parrinello, M.; Rahman, A. Polymorphic transitions in single crystals: A new molecular dynamics method. *Journal of Applied physics* **1981**, *52*, 7182–7190.

(104) Nosé, S.; Klein, M. Constant pressure molecular dynamics for molecular systems. *Molecular Physics* **1983**, *50*, 1055–1076.

(105) Fried, S. D.; Boxer, S. G. Measuring electric fields and noncovalent interactions using the vibrational Stark effect. *Accounts of chemical research* **2015**, *48*, 998–1006.

(106) Bagchi, S.; Fried, S. D.; Boxer, S. G. A Solvatochromic Model Calibrates Nitriles' Vibrational Frequencies to Electrostatic Fields. *Journal of the American Chemical Society* **2012**, *134*, 10373–10376, PMID: 22694663.

(107) Kim, S.; Lee, J.; Jo, S.; Brooks III, C. L.; Lee, H. S.; Im, W. CHARMM-GUI ligand reader and modeler for CHARMM force field generation of small molecules. *Journal of Computational Chemistry* **2017**, *38*, 1879–1886.

(108) Mani, T.; Grills, D. C. Nitrile Vibration Reports Induced Electric Field and Delocalization of Electron in the Charge-Transfer State of Aryl Nitriles. *The Journal of Physical Chemistry A* **2018**, *122*, 7293–7300, PMID: 30141944.

(109) Ballav, N.; Schüpbach, B.; Dethloff, O.; Feulner, P.; Terfort, A.; Zharnikov, M. Direct Probing Molecular Twist and Tilt in Aromatic Self-Assembled Monolayers. *Journal of the American Chemical Society* **2007**, *129*, 15416–15417, PMID: 18041835.

(110) Aschaffenburg, D. J.; Moog, R. S. Probing Hydrogen Bonding Environments: Solvatochromic Effects on the CN Vibration of Benzonitrile. *The Journal of Physical Chemistry B* **2009**, *113*, 12736–12743, PMID: 19711975.

(111) Shao, Y.; Gan, Z.; Epifanovsky, E.; Gilbert, A. T.; Wormit, M.; Kussmann, J.; Lange, A. W.; Behn, A.; Deng, J.; Feng, X. et al. Advances in molecular quantum chemistry contained in the Q-Chem 4 program package. *Molecular Physics* **2015**, *113*, 184–215.

(112) Ohno, P. E.; Chang, H.; Spencer, A. P.; Liu, Y.; Boamah, M. D.; Wang, H.-f.; Geiger, F. M. Beyond the Gouy-Chapman Model with Heterodyne-Detected Second Harmonic Generation. *The journal of physical chemistry letters* **2019**,

(113) Willets, K. A. Super-resolution imaging of SERS hot spots. *Chemical Society Reviews* **2014**, *43*, 3854–3864.

(114) Harvey, C. E.; Weckhuysen, B. M. Surface-and tip-enhanced Raman spectroscopy as operando probes for monitoring and understanding heterogeneous catalysis. *Catalysis letters* **2015**, *145*, 40–57.

(115) Sarkar, S.; Maitra, A.; Banerjee, S.; Thoi, V. S.; Dawlaty, J. M. Electric Fields at Metal–Surfactant Interfaces: A Combined Vibrational Spectroscopy and Capacitance Study. *The Journal of Physical Chemistry B* **2020**, *124*, 1311–1321.

(116) Pennathur, A. K.; Voegtle, M. J.; Menachekanian, S.; Dawlaty, J. M. Strong Propensity of Ionic Liquids in Their Aqueous Solutions for an Organic-Modified Metal Surface. *The Journal of Physical Chemistry B* **2020**, *124*, 7500–7507.

Graphical TOC Entry